ELSEVIER

Contents lists available at ScienceDirect

Composites Part B

journal homepage: www.elsevier.com/locate/compositesb





Vitrimer based composite laminates with shape memory alloy Z-pins for repeated healing of impact induced delamination

John Konlan^a, Patrick Mensah^a, Samuel Ibekwe^a, Karen Crosby^a, Guoqiang Li^{a,b,*}

- ^a Mechanical Engineering Department, Southern University and A&M College, Baton Rouge, LA, 70803, USA
- ^b Mechanical & Industrial Engineering Department, Louisiana State University, Baton Rouge, LA, 70803, USA

ARTICLE INFO

Keywords:

- A. Smart materials
- A. Recycling
- B. Delamination
- B. Impact behavior

ABSTRACT

Owing to their unique and outstanding in-plane properties and high specific strength and stiffness, fiberreinforced polymer composite laminates are being used widely for many structural applications, such as aircrafts, infrastructure, and automobiles. Notwithstanding, they are normally susceptible and vulnerable to damage from out-of-plane impact events. Low velocity impact of fiber-reinforced composite laminates often results in damages that are invisible, but would progressively propagate and later results in a catastrophic failure. This study focused on developing a self-healing composite laminate with improved transverse strength and cyclic healing capabilities that would address the problem of delamination. A novel self-healable and recyclable vitrimer-based shape memory polymer (VSMP) was used as the matrix, unidirectional Saertex glass fiber as the reinforcing fibers, and tension programmed shape memory alloy (SMA) wires (Flexinol) as z-pins. This design followed the strategy of close-then-heal (CTH) for delamination healing. Low velocity impact tests, compression after impact tests, and self-healing of impact induced delamination were investigated. The tension programmed SMA z-pins helped resist delamination during impact; the shape memory effect of the vitrimer and SMA z-pins, together with the external pressure used, helped narrow/close the delamination through constrained shape recovery during heating, so that the narrowed/closed delamination can be healed repeatedly by the VSMP itself. The novel hybrid composite laminate provides a promising sustainable multifunctional material system for structural application.

1. Introduction

Functional recovery and restoration through self-healing of damaged-polymer composites have been a topic of intensive research for years [1,2]. Self-healing can be generally divided into two groups: extrinsic healing and intrinsic healing [3]. Extrinsic healing of polymers involves incorporation of external healing agent in the form of solid healing agent such as thermoplastic particles or fibers [4–7] or liquid healing agent contained in microcapsules [8–10], hollow fibers [11,12], or microvascular network [13,14]. Intrinsic healing refers to polymers that can heal itself through various novel chemistries such as ester bond [15], disulfide bond [16], urea bond [17], hydrogen bond [18], supramolecular interaction [19], and others [20].

Most of the schemes for damage healing have been successful for healing micro or sub-micro length scale cracks. For wider opened cracks, such as delamination in laminated composite due to impact, the crack surfaces must be brought in contact before extrinsic or intrinsic healing occurs. A successful strategy for this is the biomimetic two-step scheme: close-then-heal (CTH) [21,22], i.e., close or narrow the crack first through constrained shape recovery of compression programmed shape memory polymer matrix[23,24], or through constrained shape recovery of embedded tension programmed shape memory polymer fibers [25-28], artificial muscles [29,30], and shape memory alloy wires as sutures [31-37], followed by healing intrinsically or extrinsically. Owing to their unique and outstanding in-plane properties and high specific strength and stiffness, fiber-reinforced polymer composites have been used for many structural applications such as in aircrafts, automobiles and many more infrastructure utilizations. Notwithstanding, they are normally susceptible and vulnerable to impact damage from out-of-plane impact events [38]. In laminated composites, low velocity and low energy impact usually results in delamination, along with other damages such as matrix cracking, fiber/matrix interfacial debonding, and not often, fiber fracture. Among these, delamination is the major concern because it can reduce the in-plane load carrying capacity

^{*} Corresponding author. Mechanical Engineering Department, Southern University and A&M College, Baton Rouge, LA, 70813, USA. *E-mail address:* guoqiang li@subr.edu (G. Li).

significantly [39]. Unfortunately, delamination is not visible through naked eyes, and is usually inaccessible, making manual repair impossible. Although various strategies have been used to alleviate this problem, such as using z-pins in the laminates to increase the transverse shear resistance, delamination cannot be fully eliminated. Therefore, how to heal low velocity impact induced delamination in laminated composites becomes a challenging task.

The objective of this study is to design and develop a hybrid laminated composite with the ability for repeated delamination healing by following the CTH strategy. To this end, a new ultraviolet curable thermoset polymer (vitrimer) with shape memory effect and recyclability property developed by Li et al. [40,41], was used as the matrix. E-glass fiber was used as fiber reinforcement. Tension programmed shape memory alloy (SMA) wire was used as z-pins for transverse reinforcement, and for assisting in narrowing delamination. Low velocity impact test, compression after impact test, and repeated damage/healing tests were conducted. The effect of various design parameters on the impact tolerance and delamination healing efficiency was investigated.

2. Experimental methods

2.1. Raw materials and specimens preparation

Flexinol, a Shape Memory Alloy (SMA) from Dynalloy, USA having the following properties: $\rho = 6.45 \text{ g/cm}^3$, Austenite start at 52.5 °C and finish at 60.9 °C, Martensite start at 44.8 °C and finish at 32.8 °C, and a tensile strength of 1.3 GPa with a fracture strain of 7% at Martensite, was used in this study. The 0.51 mm-diameter wire was cold programmed in the Martensitic phase by applying 6% uniaxial tensile strain at a loading rate of 1 mm/min as shown in Fig. 1. The programmed SMA fibers were then cut into pins of 4 mm long and inserted into the uncured composite laminate in the transverse direction, i.e., z-pins. Saertex unidirectional E-glass fiber and mold release agent (fib-release) utilized in this study were purchased from Fiberglast, USA. The glass fiber yarn was cut into eight plys with a rectangular shape of 152.40 mm by 25.40 mm. Following Li et al. [41], Bisphenol A glycerolate dimethacrylate and a photo-initiator 2-hydroxy-2-methyl-propiophenone were acquired from Sigma-Aldrich, USA, and used without pretreatment. The epoxy resin was conditioned by dissolving 6 mL, 3% by weight of the photo-initiator (2-hydroxy-2-methyl-propiophenone) in 100 g of bisphenol A glycerolate dimethacrylate (BPAGMA). The mixture was stirred at 100 rpm at

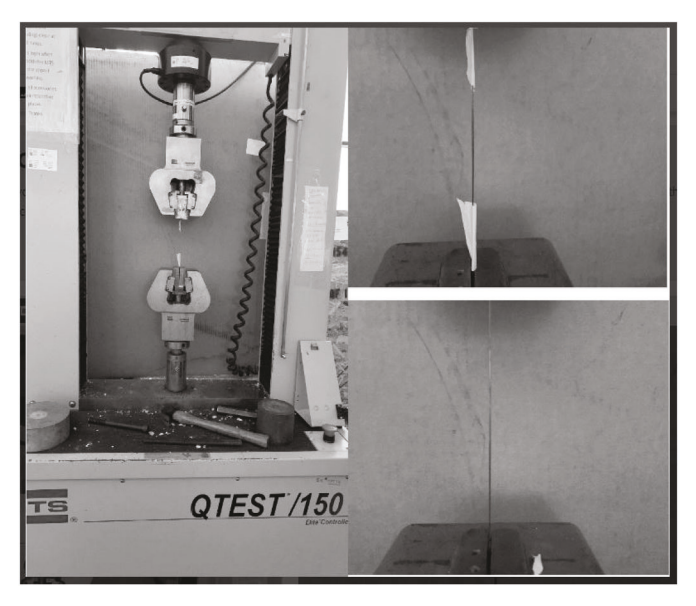


Fig. 1. Cold tension programming of flexinol SMA @ 6% strain.

75 °C for 2 h. The conditioned epoxy resin was then used to wet the glass fiber yarns. A designed 50% glass fiber volume fraction was achieved by using 8 glass fiber plys in longitudinal orientation within a 152.40 mm by 25.40 mm by 5.08 mm mold. The 4 mm SMA z-pins were then inserted into the glass fiber plys using a 3D printed guide and manually exerting a pressure of about 5 MPa using C-clamps. The volume fraction of the SMA z-pins was 2%. It is noted that the SMA z-pins were applied only in a small area of the laminate, i.e., around the center of the laminate which had an area of $25.40 \times 25.40 \text{ mm}^2$. The SMA z-pins were distributed uniformly in this region. The uncured hybrid laminate was then laid in a 3D printed mold with plain glass sheets as bottom and top covering. Thereafter, the laminate was placed in a UV chamber and readily cured at room temperature under UV-irradiation (61 mW/cm²) in 40s. Based on Li et al. [41], the cured VSMP has tensile strength of 36.7 MPa, compressive strength of 230 MPa, Young's modulus of about 3000 MPa, and fully constrained recovery stress of about 13.4 MPa. For comparisons, laminates without SMA z-pins were also prepared. For convenience, the control laminate without SMA z-pins is named as GFRP, and laminates with SMA z-pins is named as GFRP-SMA. Fig. 2 shows the fabrication process.

2.2. Programming and recovery of SMA wires

In order to investigate the shape memory effect of the SMA fibers used as z-pins in the transverse direction of the laminate, 140 mm long Flexinol wire of 0.51 mm diameter was manually cut to precise lengths and cold tension programmed at 22 $^{\circ}$ C using the MTS machine, as shown in Fig. 1. The tensile programming was performed at a loading rate of 1 mm/min until 6% strain, and was held for 15 min before unloading. The process was repeated until a sufficient number of wires was programmed. The shape fixity ratio (F_r) and shape recovery ratio (F_r) were computed using Eqs. (1) and (2), respectively:

$$F_{r} = \frac{\varepsilon_{f}}{\varepsilon_{l}} \times 100\%, \tag{1}$$

$$R_{\rm r} = \frac{\varepsilon_{\rm f} - \varepsilon_{\rm r}}{\varepsilon_{\rm f}} \times 100\%, \tag{2}$$

where ϵ_l is the strain prior to load removal, ϵ_f is the strain that has been fixed after the load is removed, and ϵ_r is the residual strain after free shape recovery.

The recovery stress of the wire was determined by clamping each of the programmed wires in the fixtures of the MTS machine in a preheated oven ($150\,^{\circ}$ C, $1.5\,$ h), to ensure that the thermal expansion of the metal fixtures in the MTS machine is avoided during data collection. With time goes by, the SMA wire is heated up to its transition temperature and tends to recover to its original shape, i.e., shrinks. Due to the constraint by the MTS machine clamps, however, this shortening in length is not allowed, creating a tensile force in the SMA wire. The recovery stress is defined as the tensile force recorded by the MTS machine divided by the cross-sectional area of the SMA wire, and the largest stress in the recovery stress-time curve is reported as the recovery stress of the SMA wire.

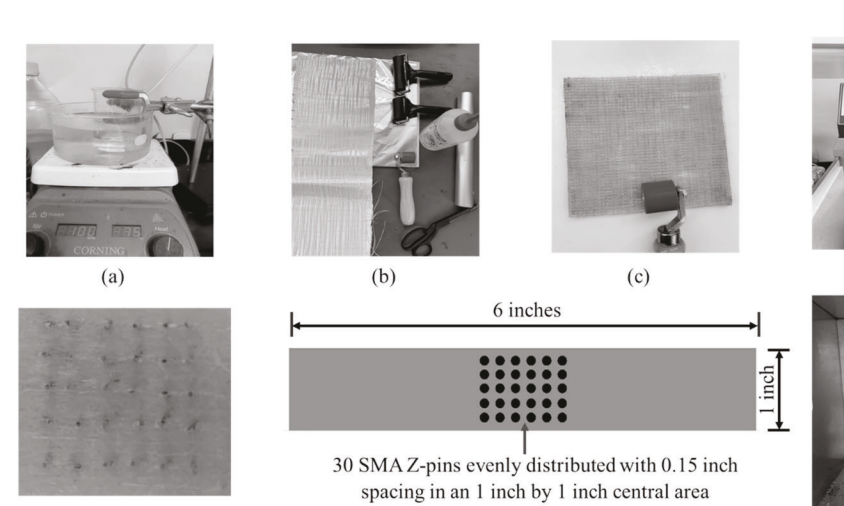
2.3. Compositional and thermomechanical analysis

The composition and degree of curing of the BPAGMA monomer and the UV-cured GFRP composite laminate were analyzed by the aid of FTIR (Bruker Alpha FTIR Spectrometer) using a scanning range from 400 to 4000 ${\rm cm}^{-1}.$

The compressive strength of the laminate, with and without the Flexinol z-pins was studied using the oven fitted MTS Machine, where the 8 mm by 8 mm by 5 mm GFRP-SMA laminate and GFRP laminate were respectively mounted in the preheated oven set at 22 $^{\circ}\text{C}$ and later at 150 $^{\circ}\text{C}$. The specimen was ramped at 0.25 mm/min until a 24% compressive strain was achieved. The elastic moduli of the samples were

(d)

(g)



(f)

Fig. 2. Composite Fabrication and Healing Procedure: (a) vitrimer preparation, (b) laying of Saertex unidirectional glass fiber, (c) rolling of vitrimer wetted glass fiber, (d) $150~\text{mm} \times 25~\text{mm} \times 5~\text{mm}$ cut-out laminate in 3D printed mold with 5~MPa pressure imposed by C-clamps in an UV curing chamber, (e) a central portion of a cured laminate with SMA z-pins, (f) schematic of SMA z-pin distributions in the laminate, and (g) set-up for delamination healing of impact damaged laminate sandwiched in between two steel plates in a MTS machine chamber.

determined.

2.4. Low velocity impact test

(e)

Instron Dynatup 8250 H V impact tester was used to carry out low velocity impact tests on the laminates according to ASTM standard D3763-18. The 152.40 mm \times 25.40 mm \times 5.08 mm specimens were impacted by a hammer weight of 11.2 kg that was dropped from a height of 205 mm. This resulted in a low impact velocity of 2 m/s. The instrumented load cell fitted to the impact tester was used to collect data in calculating the force and the absorbed energy during impact.

2.5. Compression after impact (CAI) test

CAI test was carried out on a minimum of six of the 152.40 mm \times 25.40 mm \times 5.08 mm rectangular specimens. They were tested using a strain controlled testing mode with a loading rate of 1.3 mm/min. The buckling load was used to determine the effect of damage and healing.

2.6. Recycling and healing efficiency

Vitrimer based shape memory polymers such as the Bisphenol A glycerolate dimethacrylate (BPAGMA) have appreciable recycling efficiency as demonstrated by Li et al. [41]. The healing efficiency of the laminates with and without the SMA z-pins is defined by the ratio of the crack initiation energy of the composite laminates under impact before and after healing. In addition to the crack initiation energy of the composite laminate as a basis for computing the healing efficiency, the crack propagation energy and the critical loads recorded during CAI test, were also used to ascertain the healing efficiency. The healing conditions adapted include: healing temperature at the glass transition temperature of the vitrimer at 150 °C, healing pressure of 16 MPa and healing time of 2 h. The reason of adding 16 MPa transverse pressure to the composite during healing is to help close the delamination and provide the required healing compressive stress of 14 MPa [41]. The SMA z-pins are not sufficient to provide the required compressive stress. This is because: (1) as will be discussed in Section 3.1, even under ideal assumption, i.e., each SMA z-pin provides 60 MP recovery stress, the resultant recovery force by the 30 SMA z-pins is not sufficient to achieve the required healing pressure, which is 14 MPa [41]. Assuming each SMA z-pin provides a recovery stress of 60 MPa, the maximum recovery force will be $(1/4) \times (3.14) \times (0.51 \text{ mm})^2 \times (60 \text{ MPa}) = 12.25 \text{ N}$. A total of 30 SMA z-pins were used, thus the maximum transverse compressive force provided to the laminate is $30 \times 12.25 \text{ N} = 367.52 \text{ N}$. Now the 30 SMA z-pins are distributed in an area of 25.4 mm \times 25.4 mm, thus the transvers compressive stress to the laminate is $367.52 \text{ N/}(25.4 \text{ mm})^2 =$ 0.57 MPa, which is far less than the required 14 MPa pressure for effective healing. (2) The 60 MPa recovery stress is under condition that zero recovery strain is allowed. Actually, the recovery stress decreases with recovery strain, and becomes zero at 6% recovery strain. In our study, in order to close the 34 µm delamination (see Fig. 8), the minimum recovery strain of the SMA z-pins is 0.034 mm/4 mm (SMA z-pin length) = 0.85%. Considering that the composite is not a rigid body, and will deform under this recovery stress, thus the actual recovery strain occurred in the SMA z-pins is greater than 0.85%, which leads to further reduction in the available recovery stress to close the delamination. Therefore, we used 16 MPa additional pressure to help close the delamination. Further studies are needed to enhance the delamination closing capability by SMA z-pins such as using higher volume faction of SMA z-pins, using SMA z-pins with higher recovery stress, increasing the interfacial shear strength between the polymer matrix and SMA z-pins, and using physical anchorage in SMA z-pins, or a combination of thereof.

The impacted composite laminate was sandwiched between two hard tool rectangular stainless steel plates having the same dimension as the laminate and placed in a soaked oven at $150\,^{\circ}\mathrm{C}$ for 1hr. The healing pressure was kept constant for 2 hours. This was done to achieve a higher degree of transesterification reaction of the vitrimer. The oven was turned off after the 2 hours healing period and allowed to cool to room temperature. An external air cooling source was used to shorten the cooling period. The healing efficiencies based on the crack initiation and crack propagation energy, and the CAI test is given as:

$$(\text{Healing efficiency})_{\text{I}} = \frac{E_{IR}}{E_{I0}} \times 100\%$$
 (3)

(Healing efficiency)_P =
$$\frac{E_{PO}}{E_{PP}} \times 100\%$$
 (4)

$$(\text{Healing efficiency})_{\text{CAI}} = \frac{C_{LR}}{C_{L0}} \times 100\%$$
 (5)

where subscripts I, P and CAI are notations representing healing efficiencies in terms of crack initiation energy, crack propagation energy, and compression after impact, respectively. E_{IR} , E_{PR} , C_{LR} are the crack initiation energy, crack propagation energy, and peak load of the recycled composite laminate, respectively. E_{I0} , E_{P0} , C_{L0} are the crack initiation energy, crack propagation energy and peak load of the initial composite laminate before recycling, respectively.

2.7. SEM observation

The degree of damage of the composite laminates was studied using SEM Phenom World. The surface of the damaged and healed samples studied were sputtered with gold, approximately 5 nm thick. Accelerating voltage of 10 kV was used and a working distance of 901–932 μm , with a magnification of 290 $\times \sim 300 \times$.

3. Results and discussions

3.1. Cold programmed SMA wire

The stress-strain relationship of the SMA wire under cold tension programming is shown in Fig. 3. The Flexinol SMA wire was cold programmed at 6% strain and a shape fixity ratio of 98.7% was observed by the relaxed SMA fibers. The percent loss of strain of the cold programmed Flexinol SMA fiber is 1.3%. The Elastic modulus of the cold programmed fibers was determined to be 21.5 GPa.

The recovery stress of the programmed SMA wires was 60 MPa. This stored stress in the Flexinol z-pins, when recovered, facilitate the delamination closing or narrowing, and thus healing. Fig. 4 shows the recovery stress as a function of time at the recovery temperature of 150 $^{\circ}\text{C}$. This large recovery stress provides a portion of the required force to bring the delamination surfaces in touch.

3.2. Compositional analysis

The FTIR results show that the BPAGMA monomer contained Bisphenol A unit, Ester bonds, double bonds and hydroxyl groups, as shown in Fig. 5. The wavenumbers at which these functional groups occur are at 1450 to 1600 cm⁻¹, 1735 cm⁻¹, 1680 to 1750 cm⁻¹ and 3000 to 3500 cm⁻¹, respectively. In Fig. 5, the red legend in the plot gives the absorption spectrum of the BPAGMA monomer and the black legend represents the absorption spectrum of the fully cured GFRP Composite. The strength of a composite laminate depends on the degree of curing of the vitrimer which is used as a matrix material to bind the reinforcements. From Fig. 5, it can be seen that all the double bonds are broken rigorously and completely, and they formed stronger single bonds after curing.

3.3. Impact test results

The typical load and energy traces for the GFRP and GFRP-SMA composite laminates subjected to the same low velocity impact of 2

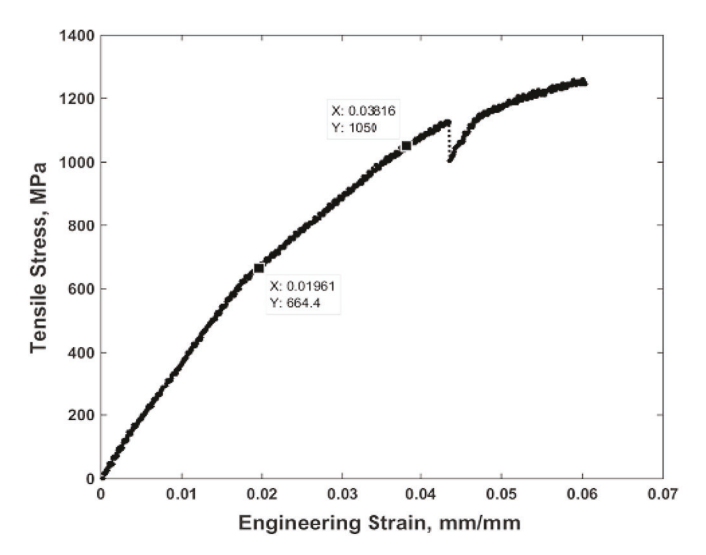


Fig. 3. Stress vs. strain for the SMA wire under tension programming.

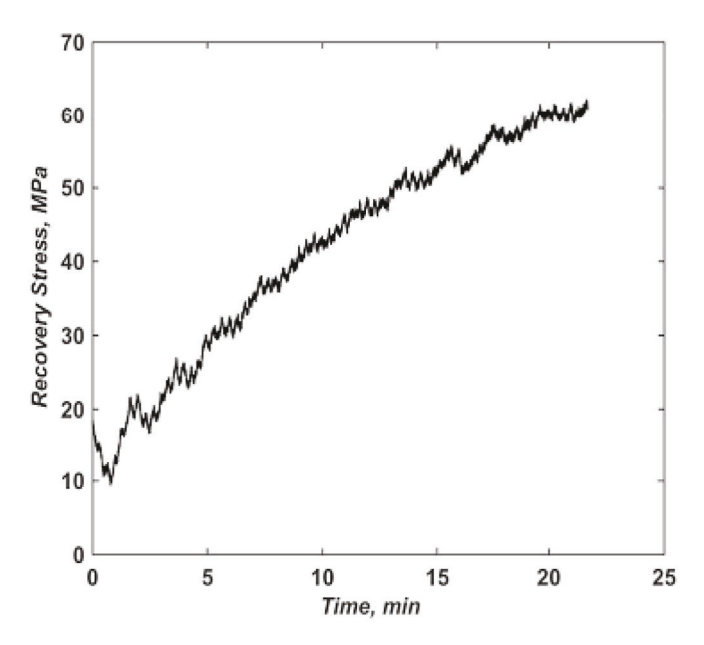


Fig. 4. Recovery stress vs. time of Flexinol wire after tension programing by 6% strain.

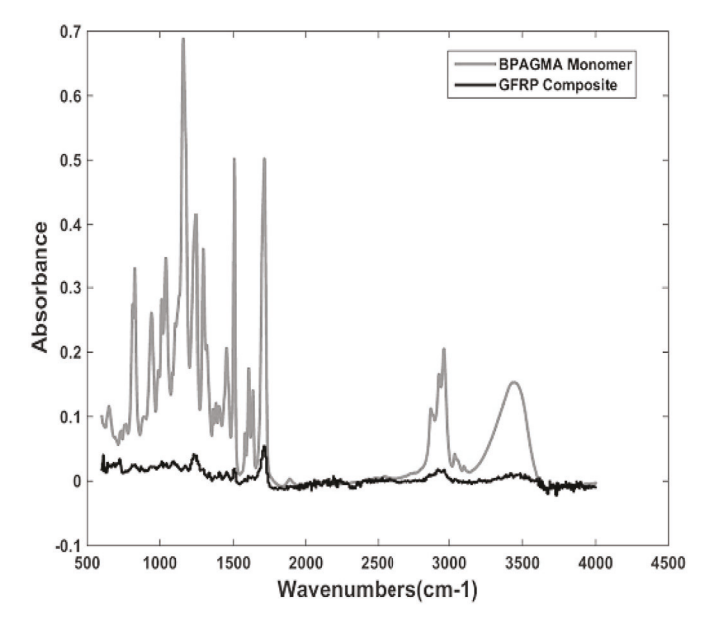
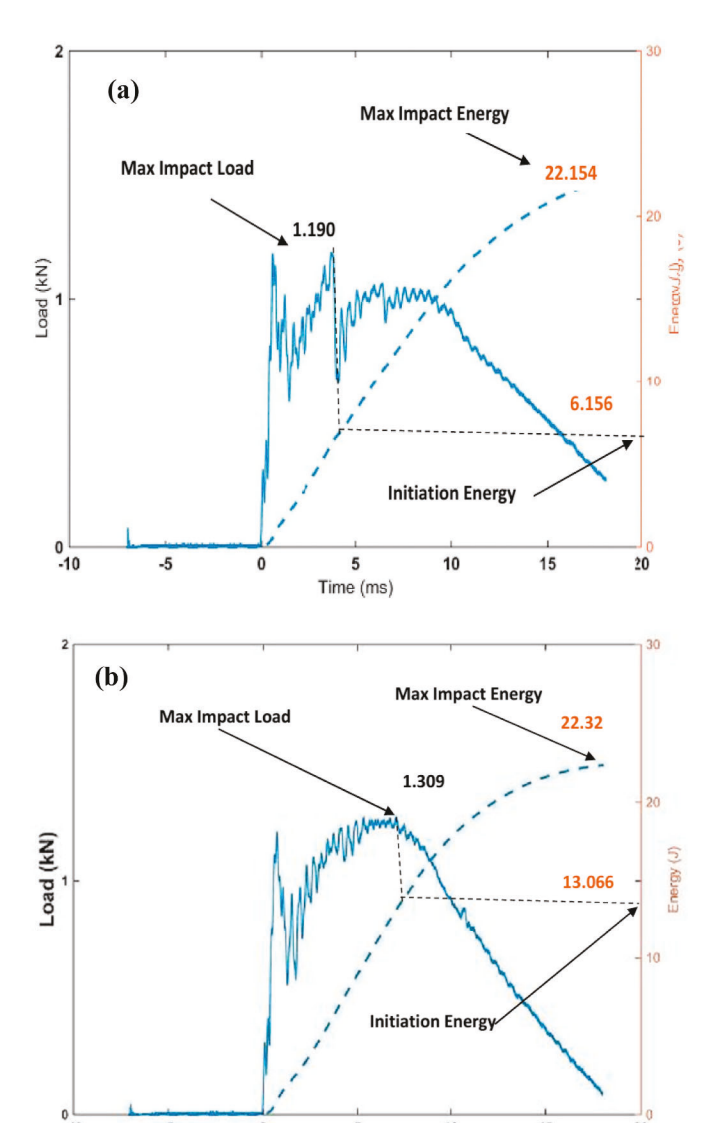


Fig. 5. FTIR spectrum of BPAGMA monomer and GFRP composite laminate, signifying complete curing of the composite laminate.

m/s with a hammer weight of 11.2 kg are analyzed in this section. In the literature, initiation energy and propagation energy are the most significant parameters to evaluate the impact tolerance of the composite laminates [42,43].

Presented in Fig. 6a and Fig. 6b are typical load-time and energy-time responses of the fabricated GFRP and GFRP-SMA laminates under low velocity impact. Table 1 summarizes the initiation energy and propagation energy obtained from the low velocity impact tests. The resistance and tolerance of the GFRP and GFRP-SMA to damage was determined using the initiation and propagation energies extrapolated from the impact test results. According to Li et al. [42,43], the initiation energy is fundamentally an indication of the capacity for a target to transfer energy elastically, and the propagation energy is the amount of energy absorbed by the target during enormous damage creation and propagation. The initiation energy is the impact energy corresponding to

J. Konlan et al. Composites Part B 200 (2020) 108324



 $\begin{tabular}{ll} Fig.~6.~a. Typical~load~and~energy~traces~of~(a)~the~GFRP-control~composite~laminate~and~(b)~the~GFRP-SMA~composite~laminate. \end{tabular}$

Time (ms)

the maximum impact force. The propagation energy is the difference between the maximum impact energy and the initiation energy [44]. Inferentially, a higher initiation energy and lower propagation energy shows the degree to which the composite laminate tolerates impact. Succinctly, the higher the initiation energy and the lower the propagation energy, the higher the impact tolerance. A higher propagation energy recorded in the test usually suggests a larger impact damage.

From Fig. 6a and b, and Table 1, the following observations can be made. (1) The SMA z-pins have significantly increased the impact tolerance as reflected by the increase in initiation energy, peak impact force, and reduction in propagation energy. (2) The significant reduction in propagation energy suggests that the SMA z-pins not only reduce the size of delamination, but also reduces the opening of the delamination,

facilitating delamination closing during healing process.

These observations can be validated by SEM images. Figs. 7 and 8(a) show the delamination of the control laminate (without SMA z-pins), and the laminate with z-pins, respectively. It is clear that the control laminate suffered from severe damage, with larger delamination and wider opening. On the contrary, the laminate with SMA z-pins experienced much smaller delamination and much narrowed delamination opening. This observation echoes the propagation energy during impact test. While the effect of z-pins on reducing delamination has been well documented [45–47], the SMA z-pins in this study provide more than delamination suppression. It will also facilitate delamination closing during the healing process, and indicating higher healing efficiency. Therefore, as compared to classical z-pins, SMA z-pins have two functionalities: suppress delamination, and facilitate delamination closing.

It is noted that SMA wires usually have very low interfacial bonding strength with thermoset polymers. This is why some previous studies used knots to physically lock the SMA wire to the polymer matrix [31–33]. In this study, however, we did not observe debonding between the SMA z-pins and the vitrimer matrix. We think this is due to a couple of reasons. (1) Comparatively low energy was used in the impact tests. (2) In previous studies [31–33], the SMA wires were mostly subjected to tensile stress, and thus it was comparatively easier for the SMA wires to be debonded or even pulled out of the matrix. In our study, the composite was under transverse impact loading, and thus the SMA z-pins immediately under impact were primarily subjected to compressive load. Due to Poisson's effect, the contact between the SMA z-pins and the surrounding matrix was even tighter. As a result, impact load did not cause interfacial debonding between the SMA z-pins and the surrounding matrix; see an image taken by an optical microscope after the first impact in Fig. 8 (b). Furthermore, using short fiber reinforced polymer theory, and assuming the maximum recovery stress of the SMA z-pin is 60 MPa, it is estimated that the interfacial shear stress between the SMA z-pins and the vitrimer matrix is less than 2 MPa, which may not be sufficient to cause interfacial debonding.

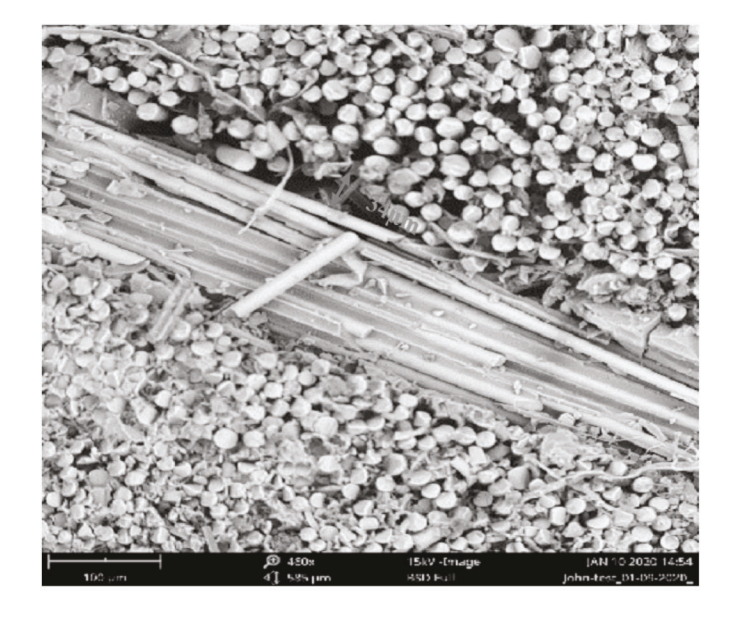


Fig. 7. SEM image of GFRP composite laminate after impact, with severe delamination.

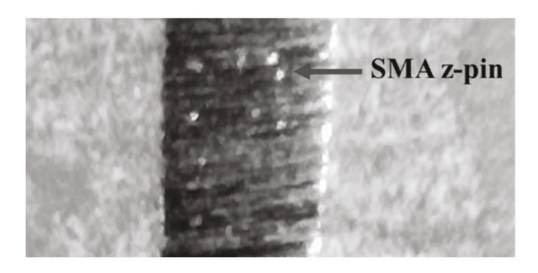
Table 1Impact test results of the laminates subjected to an impact energy of 22.4 J

Average	CD
Average	SD
1.40	0.15 0.12
	-

J. Konlan et al. Composites Part B 200 (2020) 108324



(a)



(b)

Fig. 8. (a) SEM image of GFRP-SMA Composite Laminate with minor delamination after impact; (b) Optical microscope image showing the SMA z-pin in close contact with the vitrimer matrix after first impact.

3.4. Compression after impact test

The compression after impact (CAI) test of the GFRP control and GFRP-SMA composite laminates was investigated. The critical load sustained by the various composite laminates in the compression test was used as the measurement to determine the load carrying capacity of each group of the impacted composite laminates.

Fig. 9 gives typical load – time response of the CAI test of the composite laminates. From Fig. 9, it can be seen that, the critical load for the GFRP-SMA composite laminate is about doubling that of the GFRP control laminate.

The increase in buckling resistance is due to the small delamination in the SMA z-pinned laminate. Delamination reduces the bending stiffness of the laminate, and thus buckles at lower axial load. This test again validates the role of SMA z-pins in resisting delamination propagation, and thus in increasing the CAI strength of the laminate.

3.5. Healing efficiency

It has been demonstrated before that vitrimer based shape memory polymers possess a significant recycling/healing efficiency. Li et al. [41] in their work recycled the same vitrimer. The recycling efficiency was determined by taking the ratio of tensile strength of the recycled vitrimer to the tensile strength of the original vitrimer. Recycling efficiencies

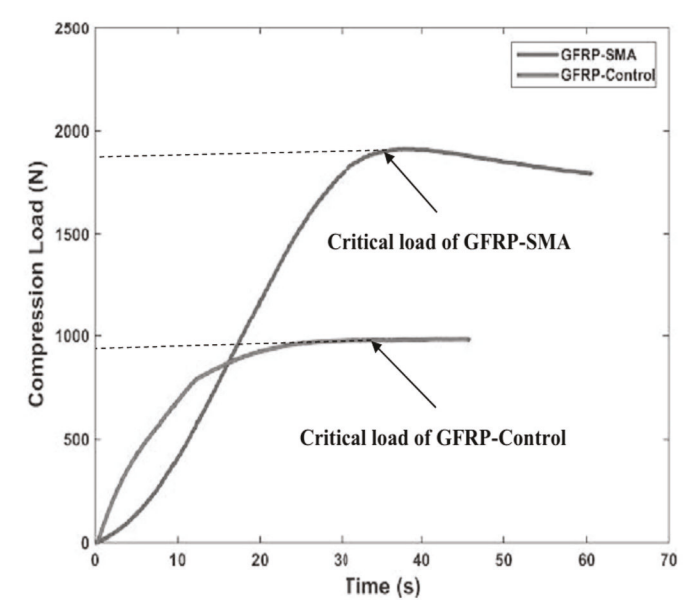


Fig. 9. Typical compression after impact test showing critical loads of GFRP and GFRP-SMA laminates.

of 69.5% and 62.1% were reported for the first and second healing cycles, respectively.

The procedure here is that the impact damaged laminates were first healed by following the CTH strategy. After healing, the specimens were tested by impact and compression after impact tests again. Three parameters were used to define the healing efficiency: crack initiation energy, crack propagation energy, and buckling load. Figs. 10 and 11 show the impact responses of the control laminate after the first and second healing cycle, respectively. Figs. 12 and 13 show the impact responses of the SMA z-pined laminates after the first and second healing cycle, respectively. Fig. 14 shows the CAI test results of the control laminate after the first impact, after the second impact, and after the third impact, respectively. Fig. 15 shows the CAI test results of the GFRP-SMA laminate after the first impact, after the second impact, and after the third impact, respectively. Fig. 16 shows the SEM images of a laminate after healing and after impact, respectively. The buckling load and healing efficiency of the GRFP-SMA and GFRP control are shown in

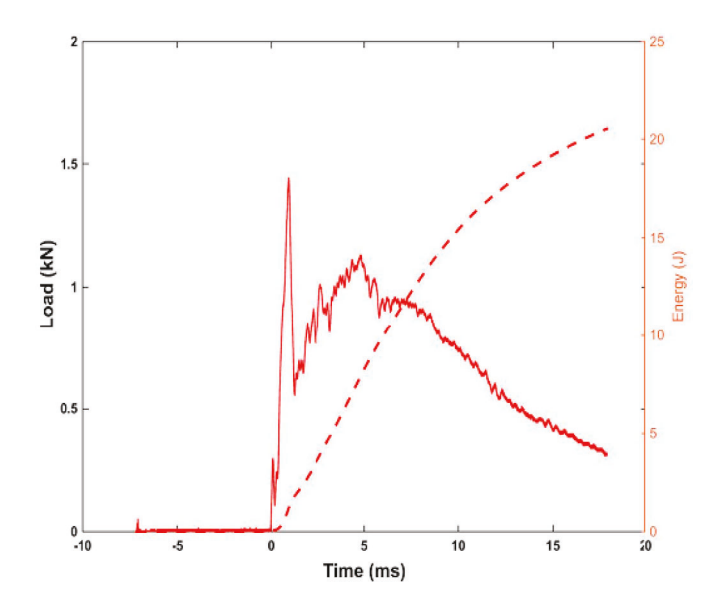


Fig. 10. Impact response of the GFRP control laminate after the 1st healing cycle.

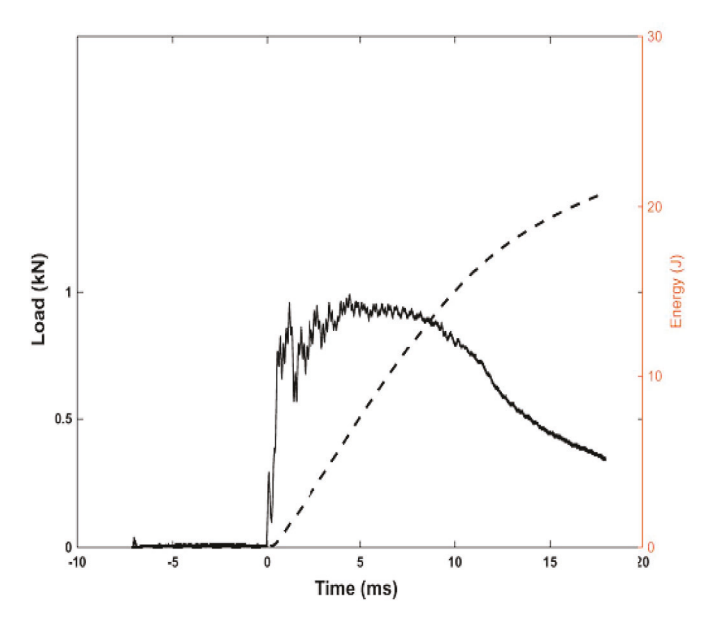


Fig. 11. Impact response of the GFRP control laminate after the 2nd healing cycle.

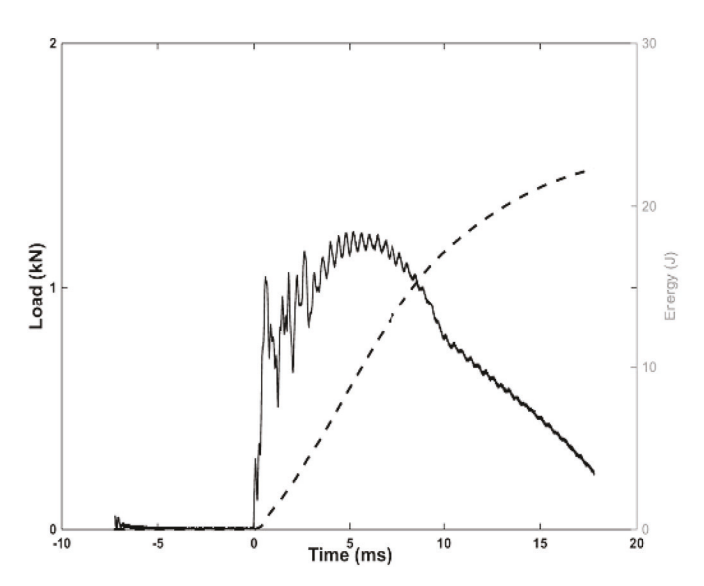


Fig. 12. Impact response of the GFRP-SMA laminate after the 1st healing cycle.

Figs. 17 and 18, respectively.

Based on the test results summarized in Table 2, and Figs. 10-18, the following observations can be made: (1) The GFRP-SMA laminates consistently show higher initiation energy, lower propagation energy, and higher buckling load than those of the control CFRP laminates, suggesting the positive effect of the small amount of SMA z-pins on enhancing the impact tolerance and residual load carrying capacity of the composite laminates. (2) The healing efficiency of the GFRP-SMA laminates basically remain unchanged as the impact/healing cycles increases, suggesting the impact tolerance can be restored repeatedly and the delamination can be fully healed. (3) The healing efficiency of the control GFRP laminates is much smaller than that of the GFRP-SMA laminates, in particular using the initiation energy as the criterion to calculate the healing efficiency. This clearly shows the advantage of using SMA as z-pins. (4) For the three healing efficiency definitions, initiation energy is comparatively sensitive to the impact/healing cycles, and thus can be used to evaluate the heling efficiency of laminated composites under impact loading. It is noted that healing efficiency can

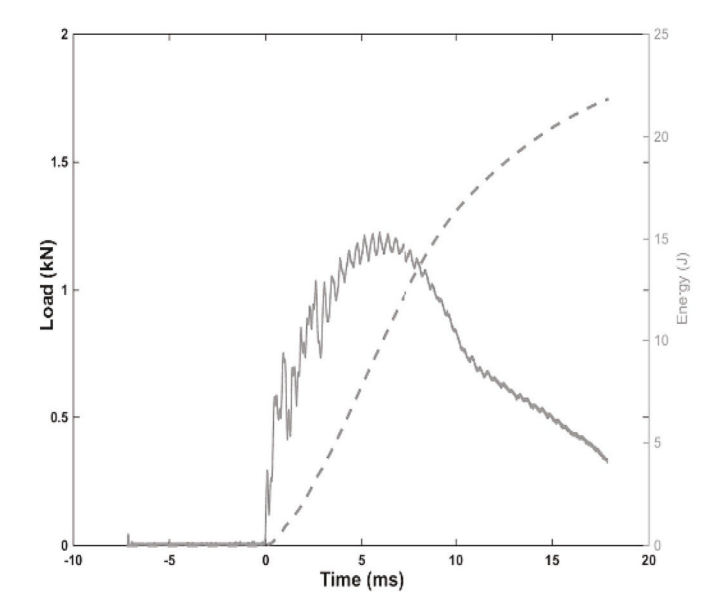


Fig. 13. Impact response of the GFRP-SMA laminate after the 2nd healing cycle.

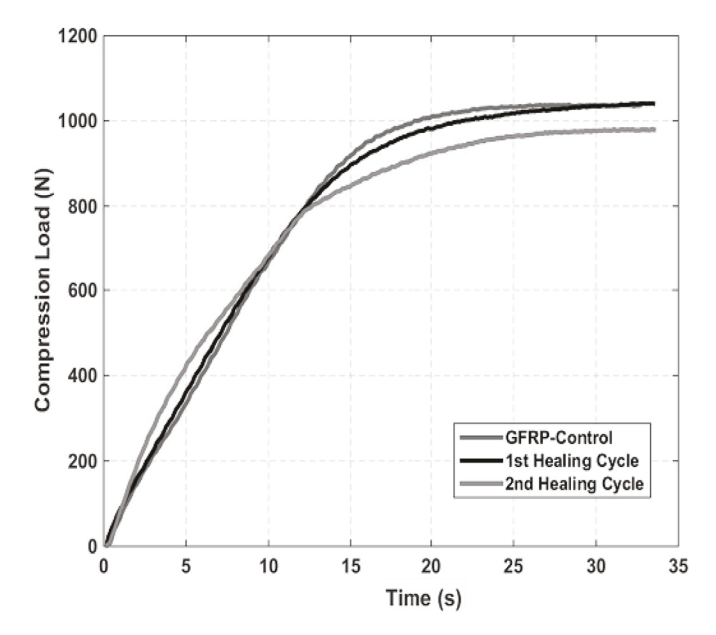


Fig. 14. Compression after impact of the GFRP control laminate after the 1st and 2nd healing cycles.

also be defined as a ratio of the damage area reduced due to healing to the damage area before healing, for example, using the area of delamination determined by non-destructive evaluation, which will be a topic in future studies.

As discussed in [40, 41], the healing efficiency of the vitrimer matrix decreases as the damage/healing cycle increases. However, from Table 2, the healing efficiency of the second healing cycle is slightly higher than or similar to that of the first healing cycle for the SMA z-pinned laminates. The reason is that the healing efficiency is affected by two competing effects in the composite. One is that the healing efficiency of the vitrimer reduces as damage/healing cycle increases [40, 41]; the other is that the coupled shape memory effect of the composite helps delamination close, and thus increases the healing efficiency. Therefore, the measured or observed healing efficiency is a result of the competitions between these two events.

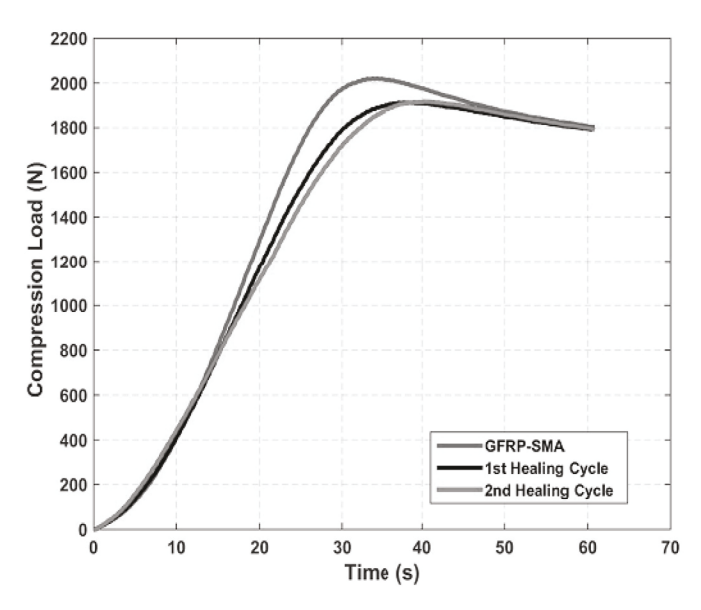


Fig. 15. Compression after impact of the GFRP-SMA laminate after the 1st and 2nd healing cycles.

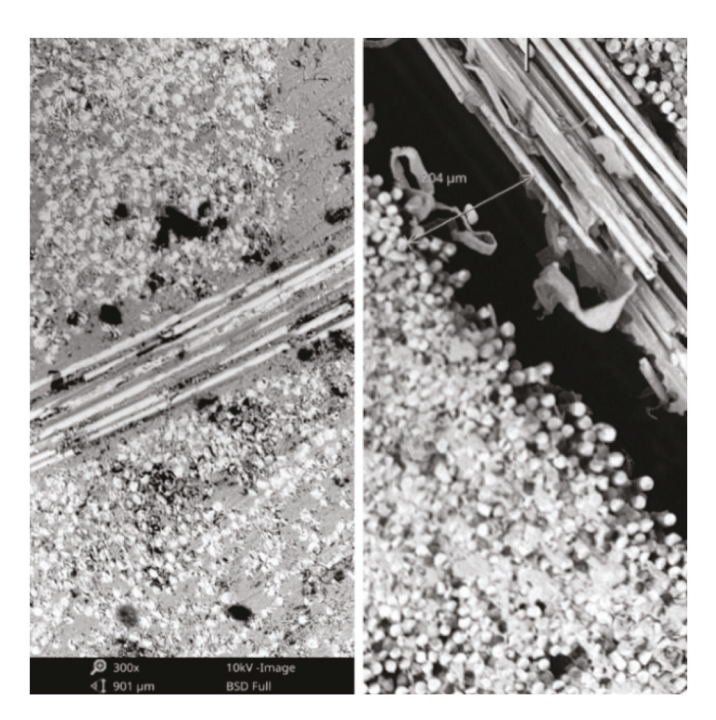


Fig. 16. Healed and unhealed delamination of the GFRP control laminate.

Now we would like to explain the effect of the coupled shape memory on the healing efficiency of the composite. As shown in [40, 41], this vitrimer is also a shape memory polymer, with a large recovery stress. For example, with 24% compression programming strain, the maximum recovery stress is 13.4 MPa [41]. In this study, the healing process is coupled with compression programming of the composite. At the healing temperature of 150 °C, the composite was compressed transversely (in the thickness direction) by a pressure of 16 MPa. After cooling and load removal, the healing is completed, which also completes the typical hot programming of the vitrimer matrix. Therefore, when comes to the second healing cycle, the compression programmed composite tends to expand in the transverse direction (recovers to its original shape). However, this expansion of the delaminated sub-laminates is resisted by the surrounding un-delaminated parts of the

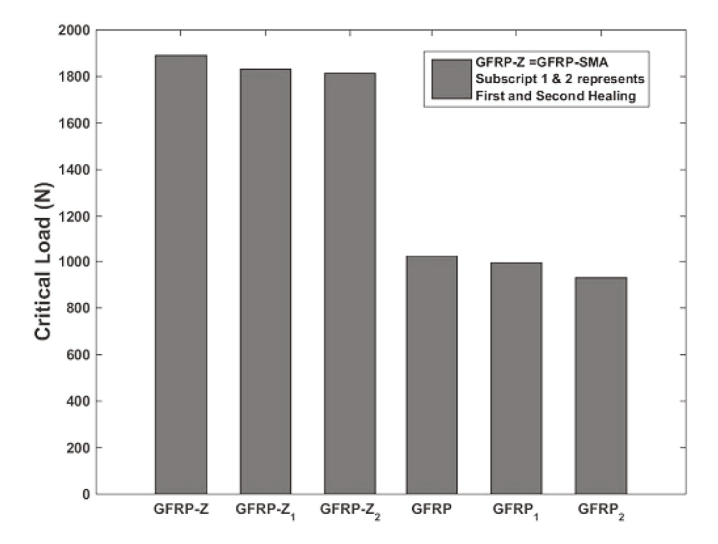


Fig. 17. Buckling loads of GFRP-SMA & GFRP control after the 1st and 2nd healing cycles.

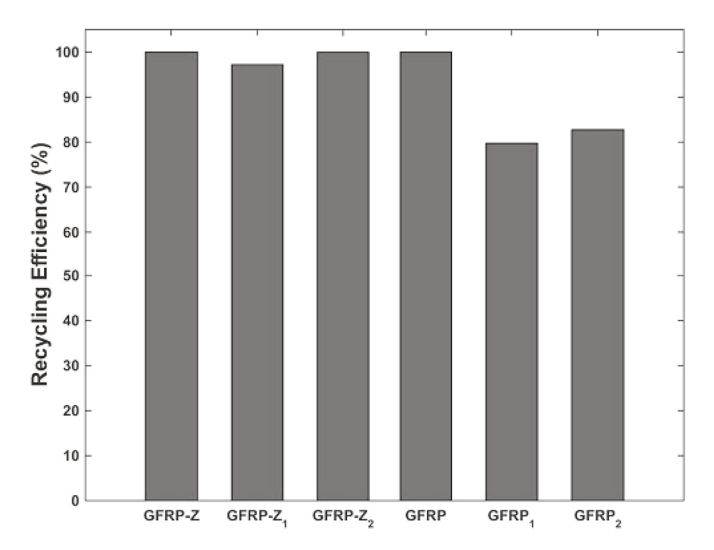


Fig. 18. Recycling efficiency of GFRP-SMA & GFRP after the 1st and 2nd healing cycles.

laminate, the un-debonded SMA z-pins, together with the 16 MPa external pressure. Consequently, the delaminated sub-laminates were pushed to the internal open space, i.e., the delamination gap, leading to tighter interfacial contact and higher healing efficiency. Therefore, the shape memory effect helps increase the healing efficiency. This conclusion has also been validated in a previous study, where curing and compression programming in the transverse direction were coupled [24]. Hence, as a result of the competition between healing efficiency reduction due to the vitrimer matrix and healing efficiency increase due to the shape memory effect, the final observed result is that the second healing cycle shows a slight increase in healing efficiency based on the initiation energy and propagation energy criteria as compared to the first healing cycle. Based on the critical buckling load criterion, however, the healing efficiency in the second cycle is slightly smaller than that in the first healing cycle.

4. Conclusions

One key challenge facing laminated composites persists in low velocity impact induced delamination, which, if not taken care of properly and timely, will cause premature failure of the entire structure. In this

Table 2Summary of mechanical properties and recycling efficiency after each healing cycle.

Composite Type	Healing Cycle	Crack Initiation Energy (CIE), J		Crack Propagation Energy (CPE), J		Critical Buckling Load (CBL), N Average	Recycling Efficiency (%)		
		Average	SD	Average	SD	_	CIE	CPE	CBL
GFRP-SMA	0	9.55	2.48	12.15	2.14	1890.81	100.00	100.00	100.00
	1	9.48	1.55	12.72	1.43	1831.32	99.24	95.52	96.85
	2	9.91	0.19	12.13	0.09	1813.92	103.76	100.16	95.93
GFRP-Control	0	5.49	3.73	15.61	3.00	1024.90	100.00	100.00	100.00
	1	3.09	2.54	18.17	2.75	994.59	56.28	85.91	97.04
	2	3.40	2.65	16.34	2.32	930.22	61.93	95.53	90.76

study, a hybrid composite laminate was designed, fabricated, and tested. The hybrid laminate consisted of a self-healing vitrimer as the polymer matrix, unidirectional E-glass fiber as in-plane reinforcement, and SMA z-pins as transverse reinforcement. The shape memory effect of the vitrimer and SMA z-pins, together with the external constraint applied during healing, helped achieve the close-then-heal design strategy. The test results show that SAM z-pins have significantly increased the impact tolerance, as reflected by almost doubled increase in initiation energy and in buckling load, as well as reduction in propagation energy. The SEM images show clear reduction in delamination opening with SMA zpins. The SMA z-pined laminates have exhibited repeated delamination healing capability during a couple of impact/healing cycles. With SMA z-pins, the healing efficiency remains very high during repeated damage/healing cycles. Even without the SMA z-pins, the healing efficiency is still repeatable, although at lower levels, signifying the repeatability of the transesterification of the vitrimer matrix. Of the three referenced parameters to determine the healing efficiency, the initiation energy criterion is a more sensitive parameter. It is optimistic that the synergy between the vitrimer matrix and SMA z-pins provides a new way of designing laminated composites to tolerate impact induced delamination.

Author statement

JK: Conducting experiments and original draft preparation; PM: Obtaining funding and draft editing; SI: Obtain funding, draft editing, and advising JK; KC: Draft editing; GL: Conceptualization, methodology, original draft preparation and reviewing, and Co-advising JK.

Declaration of competing interest

The authors declare that they have no known competing financial interests or personal relationships that could have appeared to influence the work reported in this paper.

Acknowledgements

The authors gratefully acknowledge the financial support by the National Science Foundation under grant number HRD 1736136, NASA and Louisiana Board of Regents under cooperative agreement NNX16AQ93A under contract number NASA/LEQSF (2016-19)-Phase3-10, NASA/CAN MSFC award, and National Science Foundation and Louisiana Board of Regents under Cooperative Agreement OIA 1946231.

References

- [1] Hornat CC, Urban MW. Shape memory effects in self-healing polymers. Prog Polym Sci 2020;102:101208.
- [2] Zhang P, Li G. Advances in healing-on-demand polymers and polymer composites. Prog Polym Sci 2016;57:32–63.
- [3] Li G. Self-healing composites: shape memory polymer based structures. West Sussex, UK: John Wiley & Sons; 2014.
- [4] Hayes SA, Jones FR, Marshiya K, Zhang W. A self-healing thermosetting composite material. Compos Appl Sci Manuf 2007;38:1116–20.
- [5] Nji J, Li G. A biomimic shape memory polymer based self-healing particulate composite. Polymer 2010;51:6021–9.

- [6] Nji J, Li G. Damage healing ability of A shape memory polymer based particulate composite with small thermoplastic contents. Smart Mater Struct 2012;21:025011.
- [7] Jony B, Roy S, Mulani SB. Fracture resistance of in-situ healed CFRP composite using thermoplastic healants. Mater Today Commun 2020;24:101067.
- [8] White SR, Sottos NR, Geubelle PH, Moore JS, Kessler MR, Sriram SR, Brown EN, Viswanathan S. Autonomic healing of polymer composites. Nature 2001;409: 704.7
- [9] Lee J, Zhang M, Bhattacharyyaa D, Yuan Y, Jayaramana K, Mai Y. Micromechanical behavior of self-healing epoxy and hardener-loaded microcapsules by nanoindentation. Mater Lett 2012;76:62–5.
- [10] Zhu D, Rong M, Zhang M. Self-healing polymeric materials based on microencapsulated healing agents: from design to preparation. Prog Polym Sci 2015;49–50:175–220.
- [11] Pang JWC, Bond IP. A hollow fibre reinforced polymer composite encompassing self-healing and enhanced damage visibility. Compos Sci Technol 2005;65:1791–9.
- [12] Trask RS, Williams GJ, Bond IP. Bioinspired self-healing of advanced composite structures using hollow glass fibres. J R Soc Interface 2007;4:363–71.
- [13] Toohey KS, Sottos NR, Lewis JA, Moore JS, White SR. Self-healing materials with microvascular networks. Nat Mater 2007:6:581–5.
- [14] Williams HR, Trask RS, Knights AC, Williams ER, Bond IP. Biomimetic reliability strategies for self-healing vascular networks in engineering materials. J R Soc Interface 2008:5:735–47.
- [15] Lu L, Fan J, Li G. Intrinsic healable and recyclable thermoset epoxy based on shape memory effect and transesterification reaction. Polymer 2016;105:10–8.
- [16] Rekondo A, Martin R, Ruiz de Luzuriaga A, Cabañero G, Grande HJ, Odriozola I. Catalyst-free room-temperature self-healing elastomers based on aromatic disulfide metathesis. Materials Horizon 2014;1:237–40.
- [17] Zechel S, Geitner R, Abend M, Siegmann M, Enke M, Kuhl N, Klein M, Vitz J, Gräfe S, Dietzek B, Schmitt M, Popp J, Schubert US, Hager MD. Intrinsic self-healing polymers with a high E-modulus based on dynamic reversible urea bonds. NPG Asia Mater 2017;9:e420.
- [18] Zhang A, Yang L, Lin Y, Yan L, Lu H, Wang L. Self-healing supramolecular elastomers based on the multi-hydrogen bonding of low-molecular polydimethylsiloxanes: synthesis and characterization. J Appl Polym Sci 2013;129: 2435—3442
- [19] Herbst F, Döhler D, Michael P, Binder WH. Self-healing polymers via supramolecular forces. Macromolecule Rapid Communications 2013;34:203–20.
- [20] Dahlke J, Zechel S, Hager MD, Schubert US. How to design a self-healing polymer: general concepts of dynamic covalent bonds and their application for intrinsic healable materials. Advanced Materials Interfaces 2018;5. 1800051.
- [21] Li G, Nettles D. Thermomechanical characterization of a shape memory polymer based self-repairing syntactic foam. Polymer 2010;51:755–62.
- [22] Li G, Uppu N. Shape memory polymer based self-healing syntactic foam: 3-D confined thermomechanical characterization. Compos Sci Technol 2010;70: 1419–27
- [23] Nji J, Li G. A self-healing 3D woven fabric reinforced shape memory polymer composite for impact mitigation. Smart Mater Struct 2010;19:035007.
- [24] Li G, John M. A self-healing smart syntactic foam under multiple impacts. Compos Sci Technol 2008;68:3337–43.
- [25] Zhang P, Ogunmekan B, Ibekwe S, Jerro D, Pang S, Li G. Healing of shape memory polyurethane fiber-reinforced syntactic foam subjected to tensile stress. J Intell Mater Syst Struct 2016;27:1792–801.
- [26] Li G, Zhang P. A self-healing particulate composite reinforced with strain hardened short shape memory polymer fibers. Polymer 2013;54:5075–86.
- [27] Li G, Ajisafe O, Meng H. Effect of strain hardening of shape memory polymer fibers on healing efficiency of thermosetting polymer composites. Polymer 2013;54: 920–8.
- [28] Li G, Meng H, Hu J. Healable thermoset polymer composite embedded with stimuli-responsive fibers. J R Soc Interface 2012;9:3279–87.
- [29] Zhang P, Li G. Healing-on-demand composites based on polymer artificial muscle. Polymer 2015;64:29–38.
- [30] Zhang P, Li G. Fishing line artificial muscle reinforced composite for impact mitigation and on-demand damage healing. J Compos Mater 2016;50:4235–49.
- [31] Kirkby EL, Rule JD, Michaud VJ, Sottos NR, White SR, Månson JE. Embedded shape-memory alloy wires for improved performance of self-healing polymers. Adv Funct Mater 2008;18:2253–60.
- [32] Kirkbya EL, Michauda VJ, Månsona JAE, Sottosb NR, White SR. Performance of self-healing epoxy with microencapsulated healing agent and shape memory alloy wires. Polymer 2009;50:5533–8.

- [33] Neusera S, Michauda V, White SR. Improving solvent-based self-healing materials through shape memory alloys. Polymer 2012;53:370–8.
- [34] Wang CC, Ding Z, Purnawali H, Huang WM, Fan H, Sun L. Repeated instant self-healing shape memory composites. J Mater Eng Perform 2012;21:2663–9.
- [35] Cohades A, Hostettler N, Pauchard M, Plummer CJG, Michaud V. Stitched shape memory alloy wires enhance damage recovery in self-healing fibre-reinforced polymer composites. Compos Sci Technol 2018;161:22–31.
- [36] Saeedi A, Shokrieh MM. A novel self-healing composite made of thermally reversible polymer and shape memory alloy reinforcement. J Intell Mater Syst Struct 2019;30:1585–93.
- [37] Suslu H, Fan J, Ibekwe S, Jerro D, Mensah P, Li G. Shape memory alloy reinforced vitrimer composite for healing wide-opened cracks. Smart Mater Struct 2020;29: 065008
- [38] Ibekwe SI, Mensah PF, Li G, Pang SS, Stubblefield MA. Impact and post impact response of laminated beams at low temperatures. Compos Struct 2007;79:12–7.
- [39] Pang SS, Li G, Helms JE, Ibekwe SI. Influence of ultraviolet radiation on the low velocity impact response of laminated beams. Compos B Eng 2001;32:521–8.

- [40] Li A, Challapalli A, Li G. 4D printing of recyclable lightweight Architectures using high recovery stress shape memory polymer. Sci Rep 2019;9:7621.
- [41] Li A, Fan J, Li G. Recyclable thermoset shape memory polymers with high stress and energy output via facile UV-curing. J Mater Chem A 2018;6:11479–87.
- [42] Li G, Muthyala VD. Impact characterization of sandwich structures with an integrated orthogrid stiffened syntactic foam core. Compos Sci Technol 2008;68: 2078–84
- [43] Li G, Chakka VS. Isogrid stiffened syntactic foam cored sandwich structure under low velocity impact. Compos A Appl Sci Manuf 2010;41:177–84.
- [44] Agarwal BD, Broutman LJ, Chandrashekhara K. Analysis and performance of fiber composites. third ed. Hoboken, New Jersey: John Wiley & Sons; 2006.
- [45] Partridge IK, Cartié DDR. Delamination resistant laminates by Z-Fiber® pinning: Part I manufacture and fracture performance. Compos A Appl Sci Manuf 2005;36: 55–64.
- [46] Pingkarawat K, Mouritz AP. Improving the mode I delamination fatigue resistance of composites using z-pins. Compos Sci Technol 2014;92:70–6.
- [47] Mouritz AP. Review of z-pinned composite laminates. Compos A Appl Sci Manuf 2007;38:2383–97.